Static and dynamic correlations in fluids with internal quantum states: Computer simulations and theory

P. de Smedt,* P. Nielaba, J. L. Lebowitz,† and J. Talbot‡
Department of Math, Rutgers University, New Brunswick, New Jersey 08903

L. Dooms
Instituut voor Theoretische Fysica, Katholieke Universiteit Leuven, Celestijnenlaan 200D, B-3030, Belgium
(Received 11 December 1987)

We continue our investigation of the properties of a model fluid whose molecules have classical translational degrees of freedom and two quantum internal states. The attractive pair interactions are "turned on" when the internal states are hybridized, corresponding to the molecules acquiring a "dipole" moment. The phase diagram of this system in the temperature-density plane as well as the static and imaginary-time correlations at various densities are investigated by Monte Carlo simulations, using the "polymer" representation, for different strengths of the quantum parameter. These are compared with low-density expansions and mean-field-theory predictions. Good agreement is found in appropriate regimes.

I. INTRODUCTION

In this paper we continue our study of a model-fluid system: classical particles with quantum internal degrees of freedom. This model has a long history; see Refs 1–4, which we refer the reader for motivation and background. The version we consider is the same as in our previous work:[5] a system of particles (molecules) whose relevant internal states can be represented by a two-level tunneling system, while their translations can be treated classically. We ignore all other degrees of freedom.

The N-particle Hamiltonian of the system is

$$H=\sum_{i=1}^{N}\mathbf{p}_i^2/2M-\tfrac{1}{2}\omega_0\sum_{i=1}^{N}\sigma_i^x+\sum_{\substack{i,j\\(i<j)}}U(\mathbf{r}_i-\mathbf{r}_j)-\sum_{\substack{i,j\\(i<j)}}J(\mathbf{r}_i-\mathbf{r}_j)\sigma_i^z\sigma_j^z=K+V\ , \tag{1.1}$$

where $\mathbf{p}_i$ is the momentum, M is the mass of the particles, σ^x and σ^z are the usual Pauli spin-$\frac{1}{2}$ matrices, and K and V are, respectively, the kinetic and potential energy; the latter consists of a one-particle (two-level) part and two pair-interaction terms $U(r)$ and $J(r)$, which will be specified later.

We are interested in the equilibrium properties of this system when the mass M is sufficiently large for the translational degrees of freedom to be treated classically. The classical-quantum canonical distribution function is then a product of a purely classical momentum part $\sim\exp(-\beta K)$ (which is trivial) and an N-particle density matrix μ; μ is classical, e.g., diagonal, in the coordinates $\{\mathbf{r}_i\}$ and a quantum-mechanical operator in the spin variables $\boldsymbol{\sigma}=\{\sigma_i\}$,

$$\langle\boldsymbol{\sigma}\,|\,\mu_N\,|\,\boldsymbol{\sigma}'\rangle=\langle\boldsymbol{\sigma}\,|\,\exp(-\beta V)\,|\,\boldsymbol{\sigma}'\rangle\Big/\int d\mathbf{r}_1\cdots d\mathbf{r}_N\,\mathrm{tr}_\sigma\exp(-\beta V)\ . \tag{1.2}$$

β^{-1} is the temperature.

We shall consider both the static and imaginary-time equilibrium correlation functions $\langle A(0)B(\tau)\rangle$, where A and B are operators on the spin variables, $\tau=it$, and $B(it)=e^{itV}Be^{-itV}$ (setting $\hbar=1$); $B(it)$ gives the time evolution of the spin variables at a fixed configuration $\{\mathbf{r}_i\}$. This is reasonable when M is large, so that the time scale for the internal degrees of freedom is very fast compared to the translations. We do not consider the dynamics of the classical variables $\{\mathbf{r}_i,\mathbf{p}_i\}$.

Examples of systems which can be modeled to a greater or lesser extent in this way, particularly when the positions are frozen in a regular or (quenched) disordered array, can be found in Refs. 1–9. Our mode corresponds to annealed disorder in which the positions $\{\mathbf{r}_i\}$ take on continuous values in some box Λ: we think of the particles as two-state molecules with an internal Hamiltonian $-\omega_0\sigma^x/2$, interacting via a pair potential depending on their internal state. The aim here is, however, not to mimic any particular real system but to establish reliable methods for dealing with the effects of strong interactions on the internal structure of molecules or atoms when there are no obvious collective coordinates in terms of which the description is simple. (We are particularly interested in being able to eventually treat systems such as metallic vapors, say sodium or mercury, which change as the pressure increases from a collection of weakly interacting neutral entities to a liquid metal, i.e., plasma.) For this reason we shall take $U(r)$ and $J(r)$ to have very simple forms

$$U(r)=\begin{cases}\infty, & r<R\\ 0, & r>R\ ,\end{cases}\qquad J(r)=\begin{cases}J, & R<r<\frac{3}{2}R\\ 0, & r>\frac{3}{2}R\ .\end{cases} \tag{1.3}$$

The important feature of the Hamiltonian (1.1) is that the interaction term will tend to lift particles out of their internal ground state corresponding to $\sigma^x=1$ into a hybrid state, i.e., the eigenstates of σ^z. We shall study this phenomenon as a function of β and the particle density $\rho=N/|\Lambda|$, where $|\Lambda|$ is the volume of the box Λ tak-

en to be a periodic cube (this is of no importance in the thermodynamic limit $N\to\infty$; $|\Lambda|\to\infty$; and $N/|\Lambda|=\rho$, fixed). We shall also be interested in the complementary phenomenon: how the internal quantum degree of freedom inhibits the cooperative effects of the interactions by trying to keep the particles in their ground states, where the $J(r)$ interaction vanishes. This is called "competitiveness" by Stratt[3] and leads to important modifications of the phase diagram of the system as the quantum parameter ω_0 is increased. The limit $\omega_0\to 0$ corresponds to a two-component classical system with attractive interactions $J(r)$ between particles of the same species, which favors segregation. The opposite limit, $\omega_0\to\infty$, gives a one-component classical system with only hard-core interaction $U(r)$.

While most previous analyses of these model systems were based either on mean-field theory and its extensions and/or on the use of integral equations from the theory of classical fluids (generalized to this quantum system), we follow Hall and Wolynes[4] in using computer simulations on the "equivalent" polymer model; cf. Ref. 10 for an overview. We then compare the results of the simulations with both mean-field theory and (for low density) with virial expansions in ρ.

The polymer formalism is most easily described by considering the partition function[10]

$$Z(\beta,N,\Lambda)=\lambda^{-3N}\frac{1}{N!}\int\cdots\int d\mathbf{r}_1\cdots d\mathbf{r}_N \mathrm{tr}_\sigma \exp(-\beta V)\ , \tag{1.4}$$

where λ is the de Broglie wavelength. Following Suzuki,[8] we use the Trotter formula to write Z as

$$Z=\lim_{P\to\infty}\frac{A_P^{NP}}{\lambda^{3N}N!}\int d\mathbf{r}_1\cdots d\mathbf{r}_N \exp\Big[-\beta\sum_{\substack{i,j\\(i<j)}}U(\mathbf{r}_i-\mathbf{r}_j)\Big]\times\sum_{\{S\}}\exp[-\beta\tilde{V}_P(\{S\})]\ , \tag{1.5}$$

where

$$-\tilde{V}_P(\{S\})=\sum_{i=1}^{N}\sum_{j=1}^{P}\left[K_P S_{i,j}S_{i,j+1}+\frac{1}{P}\sum_{k=i+1}^{N}J(\mathbf{r}_i-\mathbf{r}_k)S_{i,j}S_{k,j}\right],\quad S_{i,j}=\pm 1\ . \tag{1.6}$$

A_P and K_P are defined so as to make (1.5) exact for any choice of P when $J(r)=0$,

$$A_P=[\tfrac{1}{2}\sinh(\beta\omega_0/P)]^{1/2},\quad K_P=\frac{1}{2\beta}\ln[\coth(\beta\omega_0/2P)]\ , \tag{1.7}$$

and λ is the thermal wavelength. $\tilde{V}_P$ is the Hamiltonian of an Ising-like classical system of P layers. The properties of the system can now be obtained as thermal averages over the classical canonical distribution of the N times P particles,

$$\exp\left[-\beta\sum_{\substack{i,j\\(i<j)}}U(\mathbf{r}_i-\mathbf{r}_j)-\beta\tilde{V}_P(\{S\})\right]. \tag{1.8}$$

The outline of the rest of the paper is as follows. In Secs. II and III we describe the virial expansion and the mean-field theory for this system. In Sec. IV we present the results of computer simulations for a range of β and ρ at $\omega_0/2J=\frac{20}{7}$, 4, and $\frac{40}{7}$, and compare them with theory. We find that the first two terms in the virial expansion give a very good fit to all quantities for $\rho R^3\le 0.15$. The mean-field theory, on the other hand, gives some quantitative results at high density and a good qualitative picture of the overall phase diagram in the β-ρ plane. This includes both second-order and first-order phase transitions whose locations depend on the strength of the quantum parameter ω_0; see Fig. 1. We conclude in Sec. V with a discussion of the results.

II. LOW-DENSITY EXPANSIONS

A. Background

The virial expansion of the static correlation functions is, for simple classical fluids with integrable pair potentials, a well-polished subject of great formal elegance.[11] One can simply write down, in the infinite-volume (thermodynamic) limit, the coefficient of the nth power in the density ρ^n as a finite sum of specified Mayer graphs. The expansion can furthermore be shown to converge at low densities, $|\rho|<\rho_0$,[12] and so the series can be rearranged in various forms suitable for approximations.[11] The formalism generalizes to multicomponent and/or complex fluids (with internal degrees of freedom) in a straightforward way—merely requiring the piling up of indices.

The expansion formalism is more complicated and less developed for quantum fluids. Even in the absence of statistics the evaluation of the nth coefficient requires solution of the quantum-mechanical l-body problem, for all $l\le n$, including bound states, which causes many problems. Nevertheless, one can prove rigorously the convergence of the virial expansion for simple fluids using Feynman-path representations of the coefficients.[13] There are, however, more restrictions on the potentials and the bound on the density is smaller than in the classical case.

The system we are considering is intermediate between the classical and quantum case. While we are not aware of any rigorous work on the virial expansion for this type of system, many of the authors cited earlier[1-3] used formal graphical methods for the 2^P-component classical polymer system defined in (1.5). Taking the limit $P\to\infty$ is then a tricky problem: in many cases, however, it can be dealt with, at least formally. We shall not follow this line here: the correct limit, $P\to\infty$, corresponds (see Spohn and Dümke[14]) to interacting continuum Ising fields, i.e., $\sigma^x(y)=\pm 1$, for $y\in\mathbb{R}$, and explicit evaluation of higher coefficients seems difficult. Instead we shall compute the first few virial coefficients of the relevant quantities in our system directly. We do this by going back to the

definitions using the grand canonical ensemble in which the number of particles in the box Λ varies.[11] This yields an expansion of all quantities, including the density ρ, in powers of the fugacity z, which can then be manipulated to obtain an expansion in powers of ρ. This is of course also the basic starting point for classical systems. We do not, however, make any attempt to obtain a general formalism or to prove anything about convergence. That is left for the future.

B. Fugacity expansion

Given H in (1.1), we define, as usual, the density matrix at fugacity z and temperature β^{-1} as the product of the probability for there being exactly N particles in Λ times the N-particle μ given in (1.2). In obvious notation,

$$W_N=[z^N Q(N)/\Xi(\beta,z,\Lambda)]\mu_N \ , \tag{2.1}$$

where $Q(N)$ is $\lambda^{3N}Z$ given in (1.4) and Ξ is the grand partition function

$$\Xi=1+\sum_{N=1}^{\infty} z^N Q(N) \ . \tag{2.2}$$

Let us now consider the expectation value per unit volume of an operator (function) $A_l(\mathbf{r}_1,\ldots,\mathbf{r}_l;\sigma_1,\ldots,\sigma_l)$, which is symmetric in the l variables and which, for $l>1$, vanishes whenever the distance between any pair of praticles becomes large, $r_{ij}\to\infty$, $i,j\in\{1,\ldots,l\}$. We have then for a given Λ

$$\frac{\left\langle \hat{\sum} A_l \right\rangle}{|\Lambda|}=\frac{1}{l!}\sum_{N=l}^{\infty}\frac{z^N Q(N)}{\Xi}\frac{N(N-1)\cdots(N-l+1)}{|\Lambda|} \times\int\cdots\int d\mathbf{r}_1\cdots d\mathbf{r}_N \mathrm{tr}(A_l\mu_N) \ , \tag{2.3}$$

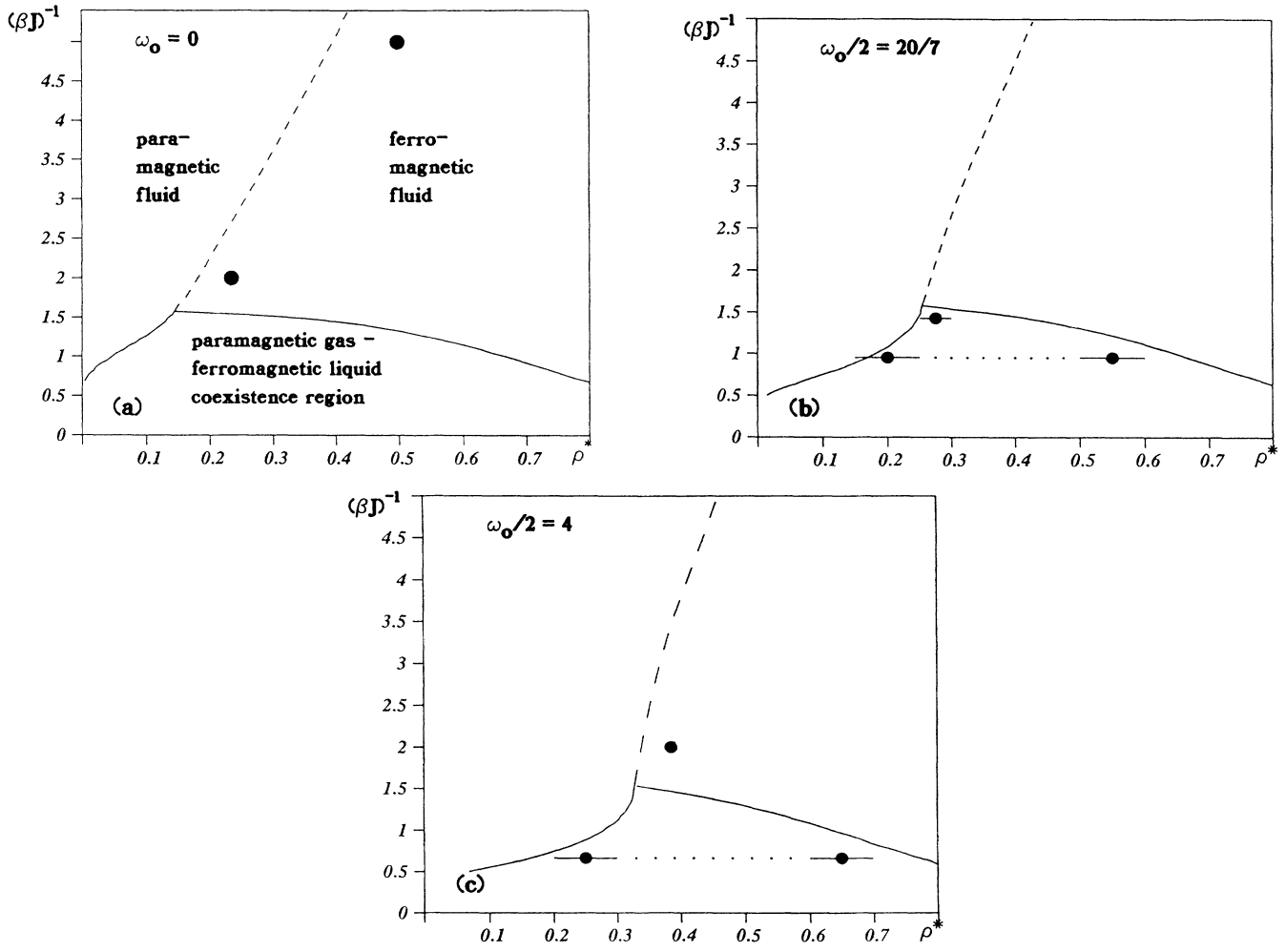

FIG. 1. Phase diagrams for $J=1$ and (a) $\omega_0/2=0$, (b) $\omega_0/2=\frac{20}{7}$, and (c) $\omega_0/2=4$. The dashed line shows the mean-field critical line for the second-order phase transition from the paramagnetic to the ferromagnetic fluid. The solid line shows the mean-field boundary of the paramagnetic-gas–ferromagnetic-liquid coexistence region for the first-order phase transition. For various values of $(\beta J)^{-1}$ the Monte Carlo transition densities (●) are shown [the values for $(\beta J)^{-1}=2$ and 5 are from Ref. 5]. In case of a first-order transition the Monte Carlo values for the boundary densities of the coexistence region are connected by dotted lines. The trend to higher values of the second-order transition densities and smaller coexistence regions continues also to $\omega_0/2=8$.

where $\hat{\sum} A_l$ means a sum over all l-tuplets in Λ.

Equation (2.3) can be expanded in the fugacity and the coefficients will have a well-defined thermodynamic limit,[10] which we shall now compute for some functions of interest. We could of course deal equivalently with the reduced density matrices, but this is more direct for our purposes.

The simplest example is $A_l=1$. The right-hand side of (2.3) is then simply the average density $\bar{\rho}(z)$, which is given simply by

$$\bar{\rho}=\lim_{|\Lambda|\uparrow\infty}\left[\frac{zQ(1)/|\Lambda|+2z^2Q(2)/|\Lambda|+\cdots}{1+zQ(1)+z^2Q(2)+\cdots}\right]=\sum_{n=1}^{\infty} nb_n z^n , \tag{2.4}$$

with

$$\begin{aligned} b_1&=[2\cosh(\tfrac{1}{2}\beta\omega_0)] ,\\ b_2&=\tfrac{1}{2}\int d\mathbf{r}_{12}\,\mathrm{tr}_{\sigma_1,\sigma_2}(\exp\{-\beta[V(1,2)]\}-\exp\{-\beta[V(1)+V(2)]\}) ,\\ b_3&=\tfrac{1}{3}\lim_{|\Lambda|\to\infty}\frac{1}{|\Lambda|}[3Q(3,\Lambda)-3Q(2,\Lambda)Q(1,\Lambda)+Q^3(1,\Lambda)] . \end{aligned} \tag{2.5}$$

In the expression for b_2 we let $\mathbf{k}$ stand for $\mathbf{r}_k$ and σ_k to show that the integrand is equal to zero when r_{12} is greater than the range of $U(r)$ and $J(r)$. In b_3 we indicated explicitly the dependence of $Q(N)$ on Λ.

The explicit evaluation of b_l essentially requires the diagonalization of V_l. This can be done readily for $l=2$ (see Ref. 15), where for a fixed r the eigenvalues of the operator

$$-\frac{\omega_0}{2}(\sigma_1^x+\sigma_2^x)-J(r)\sigma_1^z\sigma_2^z \tag{2.6}$$

are given by

$$\begin{aligned} &\lambda_1=-[J^2(r)+\omega_0^2]^{1/2},\quad \lambda_2=-J(r) ,\\ &\lambda_3=J(r),\lambda_4=[J^2(r)+\omega_0^2]^{1/2} . \end{aligned} \tag{2.7}$$

This yields

$$\begin{aligned} b_2&=\int d\mathbf{r}[e^{-\beta U(r)}(\cosh[\beta J(r)]+\cosh\{\beta[J^2(r)+\omega_0^2]^{1/2}\})-1-\cosh(\beta\omega_0)]\\ &=\int d\mathbf{r}(e^{-\beta U(r)}-1)(\cosh[\beta J(r)]+\cosh\{\beta[J^2(r)+\omega_0^2]^{1/2}\})\\ &\quad+\int d\mathbf{r}[\{\cosh[\beta J(r)]-1\}+(\cosh\{\beta[J^2(r)+\omega_0^2]^{1/2}\}-\cosh(\beta\omega_0))] , \end{aligned} \tag{2.8}$$

which reduces to the standard "classical" formulas when $J(r)=0$ or $\omega_0=0$. [For $J(r)=\omega_0=0$, $z\leftrightarrow\frac{1}{2}z$ for the purely classical fluid without internal degrees of freedom.] For the particular interactions given in (1.3), we find

$$b_2=-\tfrac{1}{2}[2\cosh(\beta\omega_0/2)]^2\tfrac{4}{3}\pi R^3+\tfrac{4}{3}\pi R^3(\tfrac{27}{8}-1)([\cosh(\beta J)-1]+\{\cosh[\beta(J^2+\omega_0^2)^{1/2}]-\cosh(\beta\omega_0)\}) . \tag{2.9}$$

We can carry out an exactly analogous expansion for σ^x or σ^z. The latter will of course yield zero for all the coefficients in the expansion (since H is invariant under $\sigma_i^z\to-\sigma_i^z$, all i), while the former gives for the average "x magnetization" per unit volume

$$\begin{aligned} \langle\sigma^x\rangle&=\sum_{i=1}^{N}\langle\sigma_i^x\rangle/|\Lambda|\\ &=[2\sinh(\beta\omega_0/2)]z+\int dr\, e^{-\beta U(r)}(4\omega_0\sinh\{\beta[J^2(r)+\omega_0^2]^{1/2}\}/[J^2(r)+\omega_0^2]^{1/2}-4\sinh(\beta\omega_0))z^2+\cdots , \end{aligned} \tag{2.10}$$

where in deriving (2.10) we had to use also the eigenfunctions corresponding to the eigenvalues given in (2.7).

A similar expansion holds for the imaginary-time-dependent correlations. Setting $\tau=it$, we define, for $0\le\tau\le\beta$, the "pseudo-one-particle" operators

$$\sigma^s(\tau)\sigma^s(0)=e^{\tau V}\sigma^s e^{-\tau V}\sigma^s,\quad s=x \text{ or } z . \tag{2.11}$$

We then have for their expectations per unit volume,

$$\begin{aligned} \tilde{C}_s(\tau)=\langle\sigma^s(\tau)\sigma^s(0)\rangle&=\sum_{i=1}^{N}\langle\sigma_i^s(\tau)\sigma_i^s(0)\rangle/|\Lambda|=\sum_{N=1}^{\infty}z^N(N/|\Lambda|)\int d\mathbf{r}_1\cdots d\mathbf{r}_N\mathrm{tr}(e^{\tau V_N}\sigma^s e^{-\tau V_N}\sigma^s\mu_N)/\Xi\\ &=\sum_{l=1}^{\infty}c_l^s(\tau)z^l,\quad 0\le\tau\le\beta . \end{aligned} \tag{2.12}$$

It is easy to check that $\tilde{C}_s(\tau)$ is symmetric about $\beta/2$. We note that

$$\tilde{\chi}_s=\beta^{-1}\int_0^\beta \tilde{C}_s(\tau)d\tau$$

is just the "self-part" of the isothermal static response function of σ^s to an external field acting on the σ^s.[16]

C. Virial expansion

To obtain an expansion in $\bar{\rho}$, we invert (2.4) to get $z(\bar{\rho})$ as a power series in $\bar{\rho}$ and substitute in (2.10) and (2.12). This yields, for the interactions (1.3),

$$\langle\sigma^x\rangle/\rho=\tanh(\beta\omega_0/2)+\rho\frac{4\pi}{3}R^3(\tfrac{27}{8}-1)[4\omega_0\sinh(\beta\lambda_4)/\lambda_4-\tanh(\beta\omega_0/2)\Gamma_+(0)]/\cosh^2(\beta\omega_0/2)+\cdots , \tag{2.13}$$

$$\begin{aligned}C_x(\tau,\rho)&\equiv\langle\sigma^x(\tau)\sigma^x(0)\rangle/\rho\\&=1+\rho\frac{4\pi}{3}R^3(\tfrac{27}{8}-1)\{\Gamma_+(\tau)\Gamma_-(\tau)/\Gamma_+(0)-\Gamma_+(0)+\omega_0^2\sinh[\lambda_4(\beta-\tau)]\sinh(\lambda_4\tau)\}/\cosh^2(\beta\omega_0/2)+\cdots ,\end{aligned} \tag{2.14}$$

$$\begin{aligned}C_z(\tau,\rho)&\equiv\langle\sigma^z(\tau)\sigma(0)\rangle/\rho\\&=[\cosh\omega_0(\beta/2-\tau)]/\cosh(\beta\omega_0/2)\\&\quad+\rho\frac{4\pi}{3}R^3(\tfrac{27}{8}-1)\{\Gamma_-(\tau)L_++\Gamma_+(\tau)L_--\Gamma_+(0)\cosh[\omega_0(\beta/2-\tau)]/\cosh(\beta\omega_0/2)\}/\cosh^2(\beta\omega_0/2)+\cdots ,\end{aligned} \tag{2.15}$$

where we have dropped the overbar from ρ and put

$$\Gamma_\pm(\tau)=\cosh\left[(\lambda_4\pm\lambda_3)\left[\frac{\beta}{2}-\tau\right]\right]\cosh\left[(\lambda_4\mp\lambda_3)\left[\frac{\beta}{2}\right]\right],\quad L_\pm=(\lambda_4\pm\lambda_3)/[(\lambda_4\pm\lambda_3)^2+\omega_0^2] .$$

The terms on the right-hand sides of (2.13)–(2.15) represent the averages per particle, which we compare in Fig. 2(a) with the results of computer simulations carried out at fixed density; see Sec. IV for details. We see that the agreement is extremely good for $\rho^*=\rho R^3\leq 0.15$, even though we used only the first two virial coefficients. Remarkably enough, we can use the formula in the square brackets (2.14) and (2.15) with ρ replaced by an adjustable parameter $a_s(\rho)$ to fit our simulations up to much higher densities. This can be seen in Fig. 3, where we plot the "self-susceptibility" $\tilde{\chi}_s(\rho)$, defined by

$$\tilde{\chi}_s(\rho)=\beta^{-1}\int_0^\beta\tilde{C}_s(\tau,\rho)d\tau , \tag{2.16}$$

as a function of ρ^*. Using the first two terms in formulas (2.14) and (2.15) with ρ replaced by a_s, we obtain from (2.16)

$$\tilde{\chi}_s(\rho)=\phi_s+a_s(\rho)\psi_s , \tag{2.17}$$

where ϕ_s and ψ_s are independent of ρ,

$$\phi_x=1 ,$$

$$\phi_z=(\beta\omega_0/2)^{-1}\tanh(\beta\omega_0/2) ,$$

$$\psi_x=\frac{4\pi}{3}R^3(\tfrac{27}{8}-1)\{\sinh(\beta\lambda_4)/\beta\lambda_4+\sinh(\beta\lambda_3)/\beta\lambda_3+\omega_0^2[\cosh(\beta\lambda_4)-\sinh(\beta\lambda_4)/\beta\lambda_4]/\lambda_4^2-2\Gamma_+(0)\}/2\cosh^2(\beta\omega_0/2) ,$$

$$\psi_z=\frac{4\pi}{3}R^3(\tfrac{27}{8}-1)2[\Gamma'_-(0)L_+/\beta(\lambda_4-\lambda_3)+\Gamma'_+(0)L_-/\beta(\lambda_3+\lambda_4)-\Gamma_+(0)\tanh(\beta\omega_0/2)/\beta\omega_0]/\cosh^2(\beta\omega_0/2) .$$

Equation (2.17) can now be used to define a_s, from the computer data for $\tilde{\chi}_s(\rho)$. Doing this we find that $a_x(\rho)\simeq a_z(\rho)=a(\rho)$, which is plotted in Fig. 4: the error bars in that figure represent the mean-square deviation of the computed $C_s(\tau)$ from that given by (2.14) and (2.15) with ρ replaced by $a_s(\rho)$. We will discuss this point further in Sec. V.

We also define the pair distribution functions

$$\rho^2 g_{\gamma\delta}(r)=\frac{1}{|\Lambda|}\left\langle\sum_{\substack{i,j=1\\(i\neq j)}}\left[\frac{1+\gamma\sigma_i^z}{2}\right]\left[\frac{1+\delta\sigma_j^z}{2}\right]\delta(\mathbf{r}_{ij}-\mathbf{r})\right\rangle , \tag{2.18}$$

where $\gamma,\delta=\pm1$. In the low-density paramagnetic regime $g_{++}=g_{--}$, and we find to the lowest (zeroth) order in the

density $g^0_{\gamma\delta}(r)$,

$$g^0_{\gamma\delta}(r)=\tfrac{1}{4}e^{-\beta U(r)}\mathrm{tr}_{\sigma_1,\sigma_2}\{(1+\gamma\sigma_1^z)(1+\delta\sigma_2^z)\exp[\beta(\omega_0/2)(\sigma_1^x+\sigma_2^x)+\beta J(r)\sigma_1^z\sigma_2^z]\}/4\cosh^2(\tfrac{1}{2}\beta\omega_0)\ . \tag{2.19}$$

For the interactions (1.3) this gives $g_+=g_{++}+g_{--}$ and $g_-=2g_{+-}$,

$$g_+(r)=\begin{cases}0, & r<R\\ \{(\omega_0/2)^2e^{\beta\lambda_4}/[\lambda_4(\lambda_4-J)]+\tfrac{1}{2}e^{\beta J}+(\omega_0/2)^2e^{-\beta\lambda_4}/[\lambda_4(\lambda_4+J)]\}/2\cosh^2(\beta\omega_0/2), & R<r<\tfrac{3}{2}R\\ \tfrac{1}{2}, & r>\tfrac{3}{2}R\ ,\end{cases} \tag{2.20a}$$

$$g_-(r)=\begin{cases}0, & r<R\\ [(\lambda_4-J)e^{\beta\lambda_4}/4\lambda_4+e^{-\beta J}/2+(\lambda_4+J)e^{-\beta\lambda_4}/4\lambda_4]/2\cosh^2(\beta\omega_0/2), & R<r<\tfrac{3}{2}R\\ \tfrac{1}{2}, & r>\tfrac{3}{2}R\ .\end{cases} \tag{2.20b}$$

An interesting feature of the quantum radial distribution functions is that the discontinuity in $g_{\gamma\delta}(r)$ at $r=\frac{3}{2}R$, where $J(r)$ is discontinuous, is unlike the classical case[11] dependent on the density. The ratio of the discontinuities in $[g_\pm(r^+)/g_\pm(r^-)]$ obtained from the simulations is shown in Table I as a function of ρ^*. The agreement with that obtained from the lowest-order density term at $\rho^*\le 0.15$ is again very good.

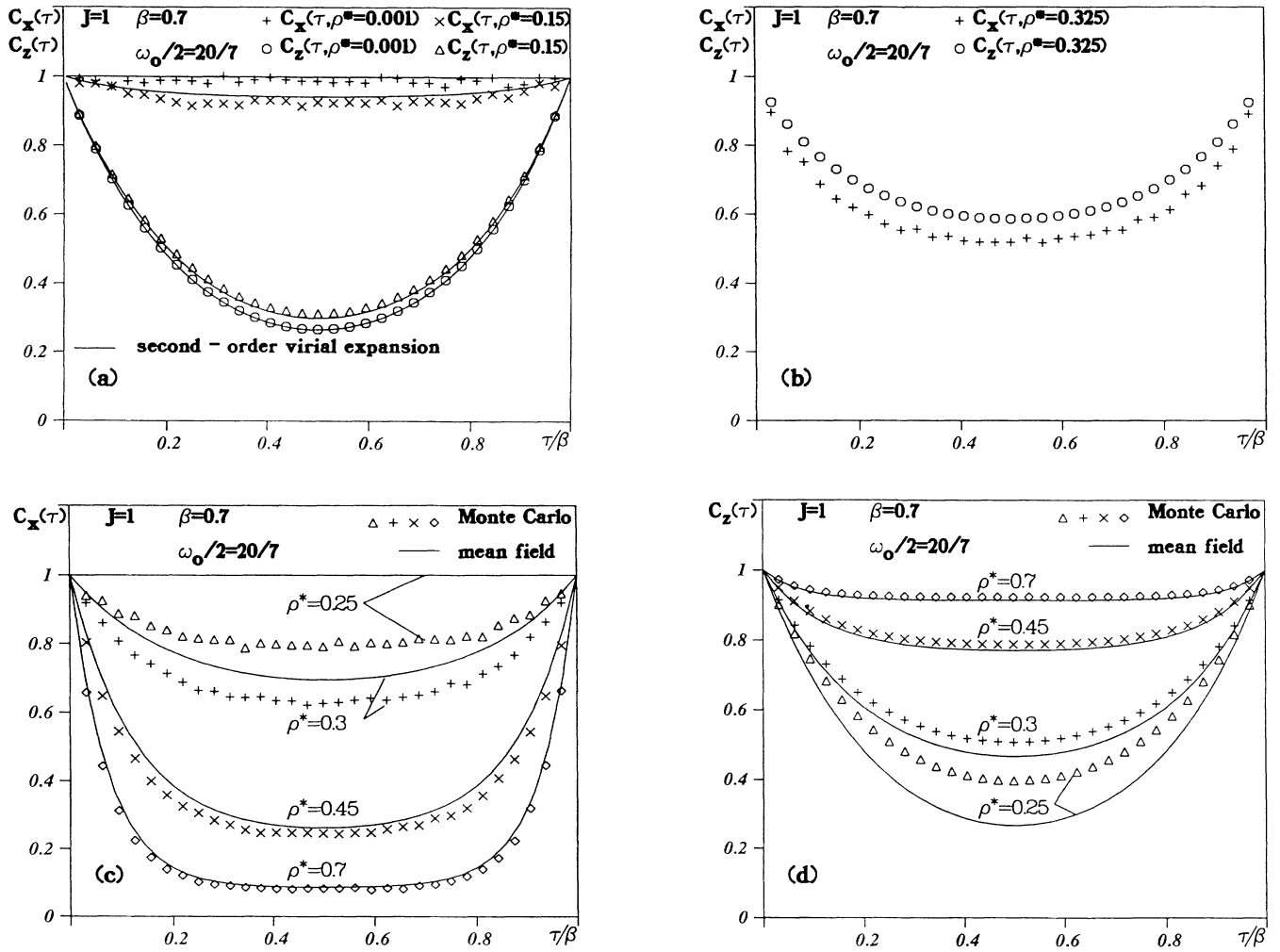

FIG. 2. Imaginary-time correlation functions. (a) and (b) Monte Carlo simulations (denoted by ○, △, +, and ×) and comparison with the second-order virial expansion. (c), (d) Comparison of Monte Carlo simulations with the mean-field theory.

The interaction energy per particle, obtained from the pair density

$$u_z=-\tfrac{1}{2}\rho\sum_{\gamma,\delta}\int J(r)\gamma\delta g_{\gamma\delta}(r)d\mathbf{r}=\rho\frac{4\pi}{3}R^3(\tfrac{27}{8}-1)(-J)[\sinh(\beta J)+J\sinh(\beta\lambda_4)/\lambda_4]/4\cosh^2(\beta\omega_0/2)+\cdots \quad (2.21)$$

is plotted in Fig. 5. Again the lowest-order term in ρ gives accurate results for small densities. We also show there the results of replacing ρ in (2.21) by $a_s(\rho)$ determined via Eq. (2.17).

III. MEAN-FIELD THEORY

The Hamiltonian of the mean-field version of our model is given by[1-3]

$$H^N_{\mathrm{MF}}=\sum_{i=1}^{N}\mathbf{p}_i^2/2M+\sum_{\substack{i,j\\(i<j)}}U(\mathbf{r}_i-\mathbf{r}_j)$$
$$-(J_0/N)\sum_{\substack{i,j\\(i<j)}}\sigma_i^z\sigma_j^z-(\omega_0/2)\sum_{i=1}^{N}\sigma_i^x\,, \quad (3.1)$$

i.e., the interaction between the internal degrees of freedom of two particles is distance independent; it decreases as $1/N$ with increasing number of particles to get a sensible thermodynamic limit.

In order to compare the results of mean-field theory with those of our model (1.1) we need to choose the value of J_0 in (3.1). Stratt (Ref. 3) takes $J_0=\rho\int d\mathbf{r}\,J(r)g(r)$, where $g(r)$ is the two-point correlation function of the underlying classical model. This is motivated as follows: In the mean-field model the magnetic field felt by, say, the first particle is

$$(J_0/N)\sum_{i(>1)}\sigma_i^z\,.$$

Assuming that the σ_i^z can be replaced by some effective value m the first spin feels an effective external field

$$(J_0/N)\sum_{i(>1)}m=J_0m$$

as $N\to\infty$. In the same spirit, we have that in our real model (1.1) the field felt by the first particle is

$$\sum_{i(>1)}J(\mathbf{r}_i-\mathbf{r}_1)\sigma_i^z\,.$$

Replacing σ_i^z by m and approximating the two-particle distribution by the classical one, we find that the effective field on any particle can be approximated by

$$m\rho\int d\mathbf{r}\,J(r)g(r)\,,$$

leading to the preceding prescription. Note that now J_0 depends on the density. Ideally, one should of course try to take the actual pair-correlation function $g(r)$ of the model. Since this is, however, not known, one takes in practice the $g(r)$ from the Percus-Yevick approximation for hard spheres. While this may not be optimal, it is the most simple and therefore the most useful for approximations. Furthermore, as seen in Fig. 6, it is in fact very close to the $g(r)$ obtained from the simulation (cf. also Sec. V).

For convenience, let us introduce an external magnetic field in our Hamiltonian,

$$H^N_{\mathrm{MF}}(h)=H^N_{\mathrm{MF}}-h\sum_{i=1}^{N}\sigma_i^z\,. \quad (3.2)$$

The properties of this system can be computed exactly in the thermodynamic limit,[3,17,18] provided one knows the properties of the classical part of the system, i.e., a system with Hamiltonian

$$H_{\mathrm{cl}}=\sum_{i=1}^{N}\mathbf{p}_i^2/2M+\sum_{\substack{i,j\\(i<j)}}U(\mathbf{r}_i-\mathbf{r}_j)\,. \quad (3.3)$$

For instance, the free energy $f(\rho;h)$ of this model in the thermodynamic limit, $\Lambda\to\infty$, $N/|\Lambda|=\rho$, is given by

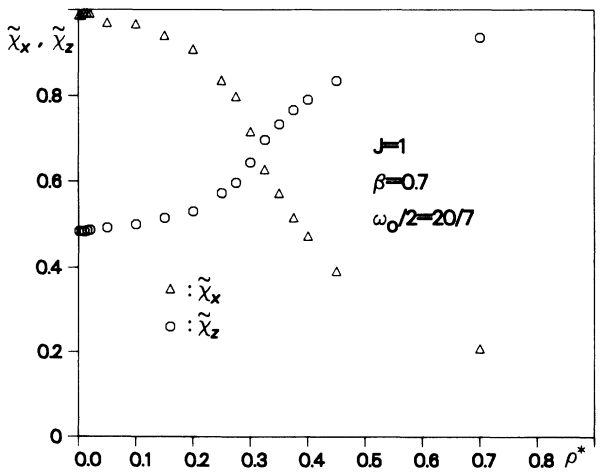

FIG. 3. "Self-susceptibility" vs reduced density. Monte Carlo simulations.

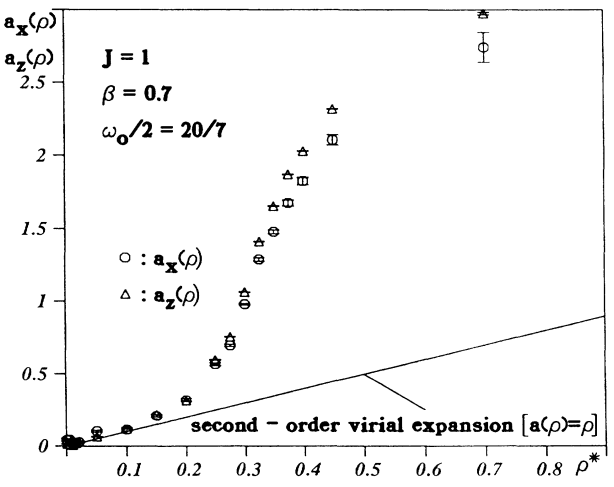

FIG. 4. Fit of $a_s(\rho)$ [see Eq. (2.17)] to the "self-susceptibility" (See Fig. 3). Comparison with the second-order virial expansion. The error bars give the least-squares error of the Monte Carlo result for $C_s(\tau)$ from that given by (2.14) and (2.15), with ρ replaced by $a_s(\rho)$.

$$f(\rho;h)\equiv\lim\frac{-1}{\beta|\Lambda|}\ln\operatorname{tr}\exp[-\beta H^N_{\mathrm{MF}}(h)]$$
$$=f_{\mathrm{cl}}(\rho)+\min_m\left[\frac{J_0\rho m^2}{2}-\frac{\rho}{\beta}\ln\cosh\{\beta[(J_0m+h)^2+(\omega_0/2)^2]^{1/2}\}\right]. \tag{3.4}$$

Here $f_{\mathrm{cl}}(\rho)$ is the free energy of a classical system with Hamiltonian (3.3) and the second term on the right-hand side of (3.4) reaches its minimum at

$$m(h)=\frac{J_0m(h)+h}{\Delta(h)}\tanh[\beta\Delta(h)]\ , \tag{3.5}$$

where

$$\Delta(h)=\{[J_0m(h)+h]^2+(\omega_0/2)^2\}^{1/2}\ .$$

For most situations, the following rule of thumb may be used: the Hamiltonian $H^N_{\mathrm{MF}}(h)$ becomes, in the thermodynamic limit $N\to\infty$, equivalent to the Hamiltonian

$$H^N(m(h);h)=\sum_{i=1}^{N}\mathbf{p}_i^2/2M+\sum_{\substack{i,j\\(i<j)}}U(\mathbf{r}_i-\mathbf{r}_j)$$
$$-\sum_{i=1}^{N}[J_0m(h)+h]\sigma_i^z-(\omega_0/2)\sum_{i=1}^{N}\sigma_i^x\ , \tag{3.6}$$

where $m(h)$ is as defined in the preceding. (In fact, the case $h=0$ is special and the statement has to be made more precise in this case.) Since the quantum-mechanical part in (3.6) is a sum of independent particle contributions, properties of this system can be calculated easily.

Let us now take a look at the solutions of (3.5). First, assume that $h=0$. For fixed J_0 and ω_0 this equation has only one solution, namely, $m=0$, for $\beta\le\beta_c$, where β_c satisfies

$$(2J_0/\omega_0)\tanh(\beta_c\omega_0/2)=1\ . \tag{3.7}$$

If $J_0<\omega_0/2$, $\beta_c=+\infty$. In this case, no phase transition occurs. If $J_0>\omega_0/2$, then for $\beta>\beta_c$ Eq. (3.5) has three solutions, namely, $m(0)$ (>0), 0, and $-m(0)$. The right-hand side reaches its minimum at $\pm m(0)$ and its maximum at zero. (The fact that the minium is reached at two points is the reason why one has to be careful in making statements about $h=0$.) When $h\neq0$, the minimum of (3.4) is reached at a unique point [although Eq. (3.5) might still have more than one solution].

Let us now look at certain specific quantities. We define

$$\langle A\rangle^h_{\mathrm{MF}}=\lim_{\Lambda\to\infty}\frac{\operatorname{tr}A\exp[-\beta H^N_{\mathrm{MF}}(h)]}{\operatorname{tr}\exp[-\beta H^N_{\mathrm{MF}}(h)]}\quad(h\neq0)\ . \tag{3.8}$$

We also define $\langle A\rangle^0_{\mathrm{MF}}=\lim_{h\downarrow0}\langle A\rangle^h_{\mathrm{MF}}$. Then, using our rule of thumb, we find

$$\langle\sigma^z\rangle^0_{\mathrm{MF}}=m(0)=\lim_{h\downarrow0}\langle\sigma^z\rangle^h_{\mathrm{MF}}\ . \tag{3.9}$$

We thus see that $\langle\sigma^z\rangle^0_{\mathrm{MF}}$ shows nonanalytic behavior when we go through the point $\beta=\beta_c$. Indeed, for $\beta\le\beta_c$, $\langle\sigma^z\rangle^0_{\mathrm{MF}}=0$, while for $\beta>\beta_c$, $\langle\sigma^z\rangle^0_{\mathrm{MF}}>0$. Moreover, one checks that for $(\beta-\beta_c)$ small that $\langle\sigma^z\rangle^0_{\mathrm{MF}}\sim(\beta-\beta_c)^{1/2}$.

We can also easily calculate $\langle\sigma_1^x\rangle^0_{\mathrm{MF}}$. We find

$$\langle\sigma_0^x\rangle^0_{\mathrm{MF}}=\begin{cases}\tanh(\beta\omega_0/2) & \text{for } \beta\le\beta_c\\ \omega_0/2J_0 & \text{for } \beta>\beta_c\ .\end{cases} \tag{3.10}$$

TABLE I. Ratio of $g_\pm(r^\mp)/g_\pm(r^\pm)$ at the potential step ($r=1.5R$, $J=1$).

		MC			
$\beta=0.7$, $\omega_0/2=\frac{20}{7}$	$\rho^*=0.2$	$\rho^*=0.3$	$\rho^*=0.4$	Eqs. (2.20)	Classical
$g_+(r^-)/g_+(r^+)$	1.36	1.54	1.75	1.27	2.01
$g_-(r^+)/g_-(r^-)$	1.15	1.07	0.88	1.15	2.01
$\beta=1.5$, $\omega_0/2=4$		$\rho^*=0.15$			
$g_+(r^-)/g_+(r^+)$		1.27		1.23	4.48
$g_-(r^+)/g_-(r^-)$		1.02		1.04	4.48
$\beta=1.05$, $\omega_0/2=3/1.05$		$\rho^*=0.15$			
$g_+(r^-)/g_+(r^+)$		1.37		1.29	2.86
$g_-(r^+)/g_-(r^-)$		1.09		1.11	2.86
$\beta=0.35$, $\omega_0/2=\frac{40}{7}$		$\rho^*=0.55$			
$g_+(r^-)/g_+(r^+)$		1.23		1.11	1.42
$g_-(r^+)/g_-(r^-)$		1.03		1.09	1.42

The susceptibility

$$\chi=\left.\frac{d\langle\sigma^z\rangle^h_{\mathrm{MF}}}{dh}\right|_{h=0}$$

can be found by differentiating expression (3.5) with respect to h. This gives for the paramagnetic region

$$\beta^{-1}\chi=\frac{[\tanh(\beta\omega_0/2)]/(\beta\omega_0/2)}{1-J_0(\rho)[\tanh(\beta\omega_0/2)]/(\omega_0/2)}\ .$$

One verifies that near β_c, $\chi\sim|\beta-\beta_c|^{-1}$. We further note that, in the mean-field model, positional correlation functions, such as

$$g(r)=\sum_{\gamma,\delta=\pm1}g_{\gamma\delta}(r)\ ,$$

are fully determined by the distance correlation functions of the underlying classical model.

We can also obtain the time-correlation functions by using our rule. We find in the limit $N\to\infty$ that

$$\lim_{h\downarrow0}\langle\sigma_i^s(0;h)\sigma_j^s(t;h)\rangle^h_{\mathrm{MF}}=\langle\sigma_i^s\rangle^0_{\mathrm{MF}}\langle\sigma_j^s\rangle^0_{\mathrm{MF}}\ , \qquad (3.11)$$

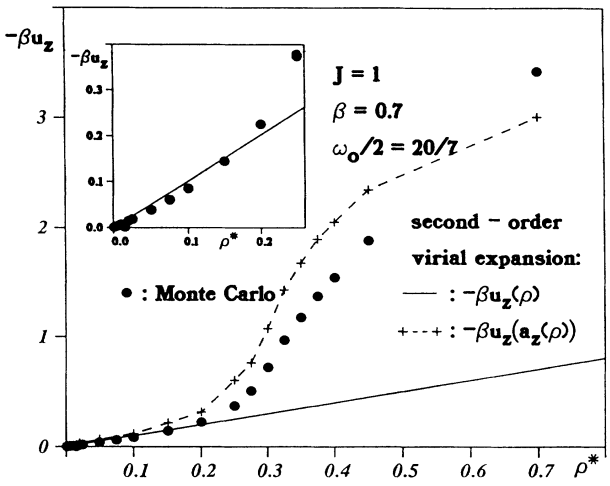

FIG. 5. Interaction energy vs reduced density. Comparison of Monte Carlo simulations and second-order virial expansion. We also show the result of replacing ρ in (2.21) by $a_s(\rho)$ determined via Eq. (2.17).

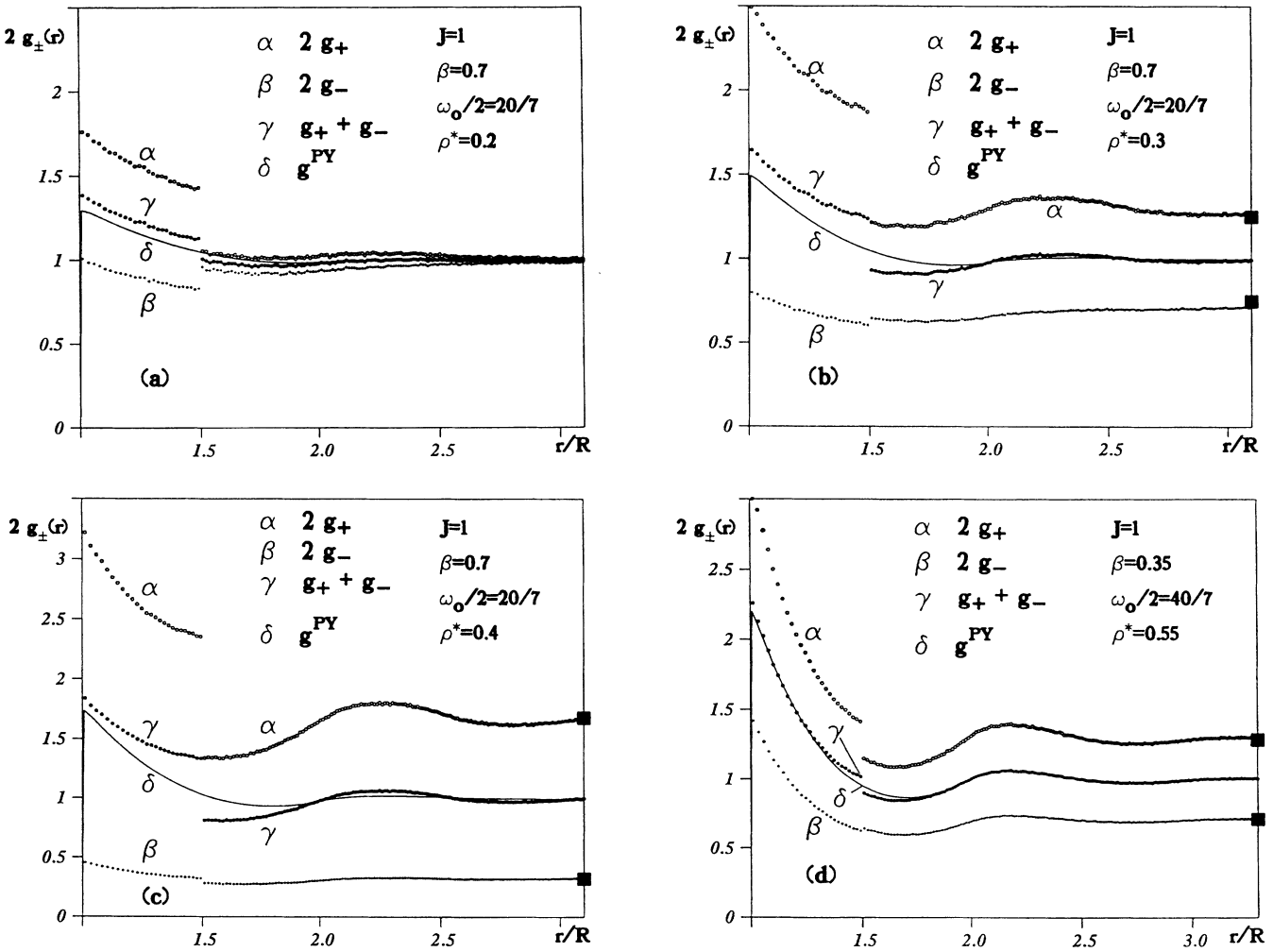

FIG. 6. Correlation functions at different densities. g^{PY} is the Percus-Yevick solution for hard spheres. The blocks at the right-hand side are at $1\pm m^2$, where m is the spontaneous magnetization obtained from the simulations; see Sec. IV B.

if $i \neq j$ and $s = z$ or x. When $i = j$ and $h = 0$ the self-correlations are given by

$$\bar{C}_z(\tau) = \frac{J_0^2 m(0)^2}{\Delta(0)^2} + (\omega_0/2)^2 \frac{1}{\Delta(0)^2} \frac{\cosh[(\beta - 2\tau)\Delta(0)]}{\cosh[\beta\Delta(0)]} \quad (0 \leq \tau \leq \beta) \quad (3.12)$$

and

$$\bar{C}_x(\tau) = (\omega_0/2)^2 \frac{1}{\Delta(0)^2} + \frac{J_0^2 m(0)^2}{\Delta(0)^2} \frac{\cosh[(\beta - 2\tau)\Delta(0)]}{\cosh[\beta\Delta(0)]} \quad (0 \leq \tau \leq \beta), \quad (3.13)$$

where, as before, $\Delta(0) = [J_0^2 m(0)^2 + (\omega_0/2)^2]^{1/2}$ and we have used a bar over the C's, defined in Eqs. (2.14) and (2.15), to indicate their mean-field nature.

In order to get the phase diagram, it is important to remember that the free energy of any physical model always needs to be a convex function of the density. This is not the case for our mean-field model. However, if the mean-field free energy contains a concave part as a function of the density, we take the convex envelope (i.e., the largest convex function which is everywhere smaller than the original function). This is nothing else than the usual Van der Waals prescription for the equation of state. The result of introducing the convex envelope is that our system now also can show first-order transitions. In Fig. 1 we have plotted the phase diagram of our system in the mean-field approximation for $\omega_0/2J = 0$, $\frac{20}{7}$, 4, and 8. At higher temperatures, the system has no phase transition when we vary the density. At lower temperatures the system undergoes, when the density is increased, a second-order phase transition from a nonmagnetized phase to a magnetized phase. Finally, at even lower temperatures the system undergoes a first-order phase transition. For a certain range of densities (region between two lines in Fig. 1), the system then splits into a low-density nonmagnetic phase and a high-density magnetic phase. Note that there would be no transition if $\omega_0/2J_0(\rho) > 1$ for any densities. In Figs. 2, 7, 8, and 9 we show how the quantities $\langle \sigma^x \rangle$, $\langle \sigma^z \rangle$, χ, and the imaginary-time-correlation functions vary when we vary the density ($J = 1$, $\beta = 0.7$, and $\omega_0/2 = \frac{20}{7}$) and compare them with Monte Carlo results. Generally, a mean-field theory should not be expected to reproduce fluctuations very well. Thus correlation functions of the form $\langle S_i S_j \rangle$ will be more accurate in the ferromagnetic regime than in the paramagnetic region, simply because the mean-field approximation that

$$\langle S_i S_j \rangle = \langle S_i \rangle \langle S_j \rangle = \langle S \rangle^2$$

contains most of the answer when $\langle S \rangle$ is not zero. In Fig. 10 we show $J_0(\rho)$—it is seen to be almost linear in ρ.

IV. MONTE CARLO SIMULATIONS

In order to study quantitatively the features of the model described by Eqs. (1.1) and (1.2), for different densities, quantum weights, and varying interaction strengths, we performed Monte Carlo simulations for fixed $J = 1$ and $R = 1$, at $\omega_0/2J = 2/0.7$, 4, 2/0.35 and

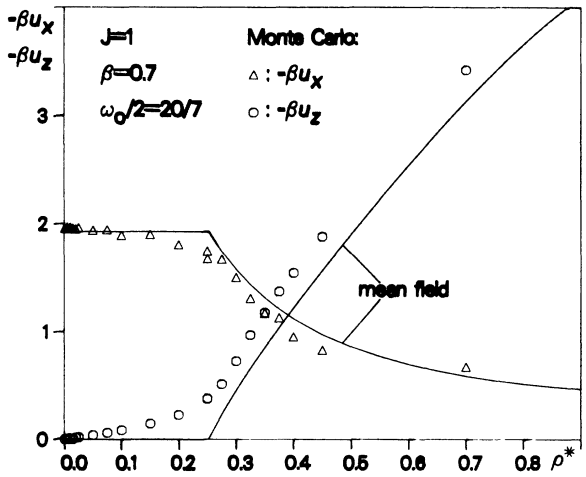

FIG. 7. Interaction and internal energy vs reduced density. Comparison of Monte Carlo simulations with mean-field theory. The interaction energy in mean-field theory is given by $\beta J_0(\rho) m^2/2$.

$\beta J = 0.7$, 1.05, and 1.5. For comparison we[5] considered purely static properties at small quantum weights ($\beta\omega_0/2 = 0, 1$, and 2 and $\beta J \approx 0.2$, 0.35, and 0.5) near the second-order transition densities. In the present work the reduced density $\rho^* = \rho R^3$ was varied up to 0.7, which is still far below the freezing density. The number of classical particles N was 100 and the number of "monomers" in the polymer P [see Eq. (1.5)] was 32, except for the case of $\omega_0/2J = 4$ and $\beta J = 1.5$, where $N = 200$ and $P = 48$. These values of P appeared sufficient for points investigated, i.e., increasing them did not seem to affect the results. The good agreement with the results of the virial expansion at low densities is further evidence of this adequacy. A typical run with 3×10^6 Monte Carlo steps took about 2 h on a Cyber 205.

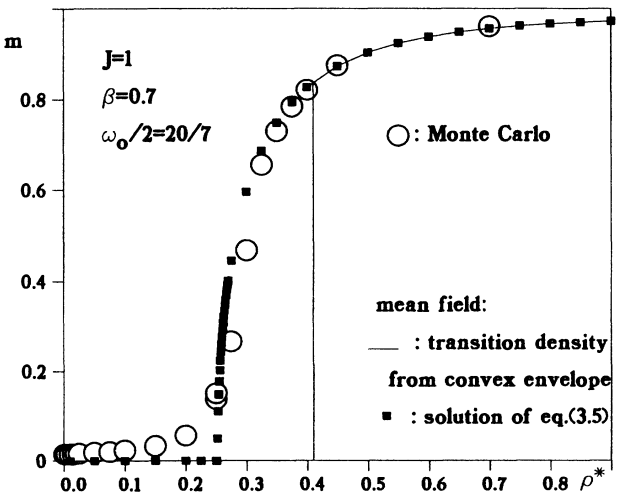

FIG. 8. Magnetization vs reduced density. Comparison of Monte Carlo simulations with the mean-field theory. The mean-field values of m, denoted by ■, to the left of the vertical line are metastable or unstable states.

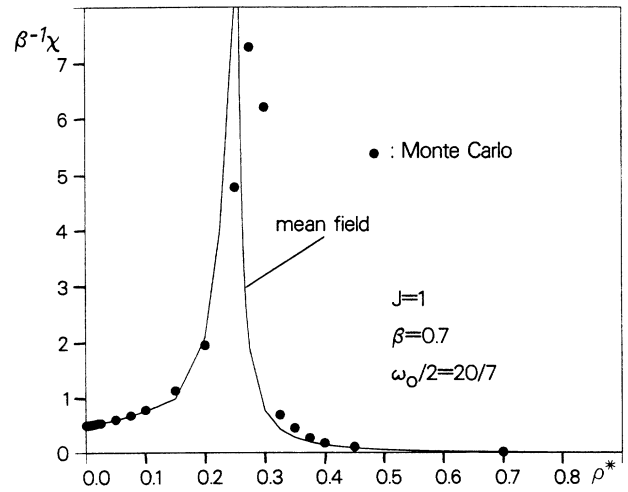

FIG. 9. Susceptibility vs reduced density. Comparison of Monte Carlo simulations with the mean-field theory.

A. Phase diagram

As already mentioned, the phase diagram is given qualitatively by mean-field theory: for small βJ the system undergoes, as ρ is increased, a second-order phase transition from the paramagnetic to the ferromagnetic phase. At larger values of βJ, a formation of clusters sets in, and the system undergoes a first-order phase transition from the paramagnetic to the ferromagnetic phase (Fig. 1). The coexistence region of the first-order transition was judged by sampling the clusters with a weak external (gravitational) field, which separates regions of high and low densities. Outside the density range of the transition the system shows no separation, whereas inside the transition range a strong tendency towards clustering can be observed. This behavior is typical for a first-order transition.

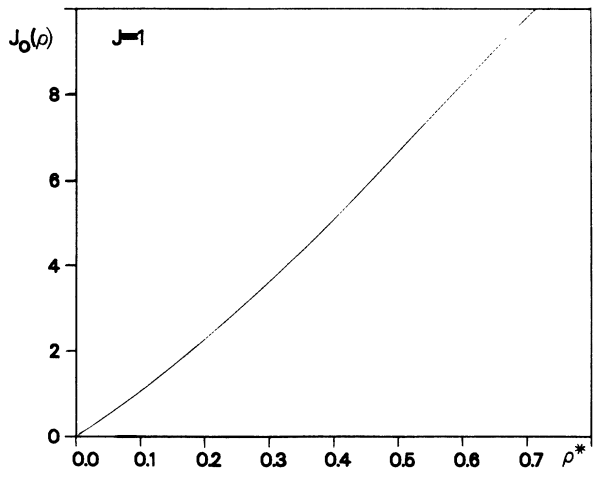

FIG. 10. $J_0(\rho)$.

B. Thermodynamic and pair correlation functions in the different phases

We computed the internal energy, using standard Monte Carlo techniques,[10] on the classical polymer system using the following definitions: the one-particle energy,

$$-\beta u^x=(\beta\omega_0/2)\left\{\tanh^{-1}(\beta\omega_0/P)-\sinh^{-1}(\beta\omega_0/P)\frac{1}{N}\times\left\langle\sum_{i=1}^{N}\frac{1}{P}\sum_{k=1}^{P}S_{i,k}S_{i,k+1}\right\rangle\right\};\tag{4.1}$$

the interaction energy,

$$-\beta u^z=\beta\frac{1}{N}\left\langle\sum_{\substack{i,j\\(i<j)}}^{N}J(|\mathbf{r}_i-\mathbf{r}_j|)\frac{1}{P}\sum_{k=1}^{P}S_{i,k}S_{j,k}\right\rangle;\tag{4.2}$$

the susceptibility (cf. Ref. 19),

$$\beta^{-1}\chi=\frac{1}{N}\left[\left\langle\left[\sum_{i=1}^{N}\frac{1}{P}\sum_{k=1}^{P}S_{i,k}\right]^2\right\rangle-\left\langle\sum_{i=1}^{N}\frac{1}{P}\sum_{k=1}^{P}S_{i,k}\right\rangle^2\right];\tag{4.3}$$

the magnetization,

$$m=\frac{1}{N}\left\langle\sum_{i=1}^{N}\frac{1}{P}\sum_{k=1}^{P}S_{i,k}\right\rangle;\tag{4.4}$$

and the pair-correlation functions $g_{\pm}(r)$ for parallel and antiparallel spins,

$$g_{\pm}(r)\equiv\frac{1}{N^2}\left\langle 2\sum_{\substack{i,j\\(i<j)}}^{N}\frac{1}{P}\sum_{k=1}^{P}\tfrac{1}{2}(1\pm S_{i,k}S_{j,k})\times\delta(|\mathbf{r}_i-\mathbf{r}_j|-r)\right\rangle.\tag{4.5}$$

We observed the following general behavior: as the density is increased there is a continuous increase of $-\beta u^z$, and a decrease of $-\beta u^x$, indicating a changeover from occupation of eigenstates of σ^x to that of σ^z, i.e., hybridization. The degree of this hybridization at a given ρ depends strongly on ω_0. The second-order transition is visible by a large increase in the susceptibility. Beyond the phase transition density the magnetization takes nonzero values approaching 1 (see Fig. 8) as ρ is increased, indicating the dominance of cooperative effects.

The pair correlation functions for higher densities show maxima at distances near multiples of the hard-sphere diameter R with intermediate minima, representing the layering structure of the classical fluid. As usual, the probabilities for finding particles with parallel spin are enhanced at close distances, compared to the uncorrelated case. The integral of the difference $\beta J\rho[g_+(r)-g_-(r)]$ over the interaction shell gives the

interaction energy; see Fig. 6.

For large distances the expectation values of $\langle \sigma_i^z \sigma_j^z \rangle$ factorize. For densities beyond the transition, i.e., in the ferromagnetic phase, the probability for finding two parallel spins at large distances is higher than for antiparallel spins, $g_+(r) > g_-(r)$, the value of the difference, for $r \to \infty$, is given by m^2; see Figs. 6.

At $r = \frac{3}{2}R$ the correlation functions are discontinuous. The deviations of the ratios of

$$g_\pm(\tfrac{3}{2}R^-)/g_\pm(\tfrac{3}{2}R^+)$$

from the classical ratios, given by the Boltzmann factors $\exp(\pm\beta J)$, may be thought of in terms of a quantum screening effect. The two-particle approximation for $g_\pm(r)$ (see Sec. II) already shows this effect of the weakened effective interaction. The agreement of the Monte Carlo (MC) results, with those obtained from the lowest terms in the virial expansion is good for low densities; see Figs. 6 and Table I. At higher densities the values for $g_\pm(\frac{3}{2}R^-)$ are enhanced. The weak discontinuity of $g_-(r)$ at $r = \frac{3}{2}R$ for high densities is in great contrast to the classical results, with only a weak dependency of the density.

C. Imaginary-time correlations

We studied the behavior of the imaginary-time correlation functions $C_z(\tau,\rho)$ and $C_x(\tau,\rho)$. These give information about the degree to which the system is in "eigenstates" of σ^x or σ^z.

We determine $C_z(l\beta/P,\rho)$ by taking the products of the spins $S_{i,j}S_{i,j+l}$ at points in the chain at a distance $l \in \{0,1,\ldots,P-1\}$ and averaging over i and j. The (unnormalized) $C_x(l\beta/P,\rho)$ is obtained by exponentiating the sum of products of neighboring pairs in ascending order, where the first of the pairs are at a distance $l\beta/P$,

$$C_z(l\beta/P,\rho) = \frac{1}{N}\left\langle \sum_{j=1}^{N} \frac{1}{P} \sum_{k=1}^{P} S_{j,k}S_{j,k+l} \right\rangle , \tag{4.6}$$

$$\begin{aligned} C_x(l\beta/P,\rho) &= \frac{1}{N}\left\langle \sum_{j=1}^{N} \frac{1}{P} \sum_{k=1}^{P} \exp[\beta K_P(-2S_{j,k}S_{j,k+1} - 2S_{j,k+l}S_{j,k+l+1})] \right\rangle \\ &= \tanh^{-2}(\beta\omega_0/P) - \tanh^{-1}(\beta\omega_0/P)\sinh^{-1}(\beta\omega_0/P) \\ &\quad \times \frac{1}{N}\left\langle \sum_{j=1}^{N} \frac{1}{P} \sum_{k=1}^{P} (S_{j,k}S_{j,k+1} + S_{j,k+l}S_{j,k+l+1}) \right\rangle \\ &\quad + \sinh^{-2}(\beta\omega_0/P)\frac{1}{N}\left\langle \sum_{j=1}^{N} \frac{1}{P} \sum_{k=1}^{P} (S_{j,k}S_{j,k+1}S_{j,k+l}S_{j,k+l+1}) \right\rangle . \end{aligned} \tag{4.7}$$

At low densities the particles are in eigenstates of σ^x, $C_x(\tau,\rho)$ is nearly 1, and $C_z(\tau,\rho)$ shows a pronounced minimum at $\tau = \beta/2$ [see Fig. 2(a)], indicating that the eigenstates of σ^z are least correlated at opposite points in the "polymer." With increasing density the system goes into hybrid states: the σ^x eigenstates are now less correlated and the tendency to more correlated σ^z eigenstates increases. $C_x(\tau,\rho)$ starts building a minimum at $\beta/2$, and the value of $C_z(\beta/2,\rho)$ increases; see Fig. 2(b). As the density crosses the phase transition between the paramagnetic and ferromagnetic phases, $C_z(\tau,\rho)$ and $C_x(\tau,\rho)$ interchange their form. $C_x(\beta/2,\rho)$ is now smaller than $C_z(\beta/2,\rho)$, corresponding to the ordering tendency of the $\sigma_i^z\sigma_j^z$ interaction. For densities above the phase transition, $C_z(\tau,\rho)$ approaches unity; see Figs. 2(c) and 2(d).

The (imaginary) -time averages of $C_z(\tau,\rho)$ and $C_x(\tau,\rho)$ over the interval between 0 and β [see Eq. (2.16)] vary only little with the density for small densities, with values of $\tilde{\chi}_x = 1$ and $\tilde{\chi}_z = 2\tanh(\beta\omega_0/2)/\beta\omega_0$ for $\rho = 0$; see Fig. 3. Near the transition density the increasing tendency towards occupations of σ^z eigenstates cause a sharp decrease of $\tilde{\chi}_x$ and increase of $\tilde{\chi}_z$, with $\tilde{\chi}_z$ and $\tilde{\chi}_x$ crossing each other. Beyond the transition density $\tilde{\chi}_z$ approaches

1. This behavior is of course very different from that of the total susceptibility χ shown in Fig. 9—the $\tilde{\chi}$ behave more like energies than like true susceptibilities.

V. DISCUSSION

We first note again that in the model treated here the translational degrees of freedom are frozen out as far as the dynamics is concerned. In particular, the (imaginary) time-dependent correlations computed here correspond to a quantum evolution of the spin variable at fixed positions, averaged over different configurations $\{\mathbf{r}_i\}$ according to the (annealed) Gibbs measure (1.2). The justification for this kind of adiabatic (Born-Oppenheimer) approximation for real systems remains to be investigated.

Given the model, some of the most interesting questions concern the interplay, or competition (cf. Ref. 3) between quantum and cooperative effects as the density is varied at a given temperature and quantum strength ω_0. For the system to take advantage of the "dipole-dipole" interactions it has to first be in a state in which it has such a moment, i.e., hybridization. Since this is unfavorable as far as the "internal" energy $-(\omega_0/2)\sigma^x$ is con-

cerned, the cooperative effects are inhibited. The larger the ω_0, the greater the density necessary for cooperativity to dominate. This can be thought of as a reduction in the effective dipole interactions with increasing ω_0, and explains qualitatively the main features of the observed behavior.

In particular, the increase of the transition density, from a paramagnetic to a ferromagnetic fluid, as ω_0 is increased (Fig. 1), can be understood in this way. In fact, in the low-density region the particles seem to be pretty much in the $\sigma^x=1$ state (cf. Fig. 7), with very little effective dipole interaction. It is presumably for this reason that the first two terms in the virtial expansion are sufficient in this region (Figs. 2, 4, and 5 and Table I). This still leaves a mystery why the scheme (2.17), which replaces the whole system by one having only the four energy levels given in (2.7), works as well as it does in Figs. 4 and 5.

Quantum mechanics also has the effect of "smearing out" of the interaction, replacing the classical point particle by a "polymer." This may explain at least in part why mean field does so well at moderate and high densities, using just the hard-sphere $g(r)$; cf Figs. 2(c), 2(d), and 7–9. An inspection of Fig. 8 shows the Monte Carlo results following rather closely the mean-field values into the metastable region of the latter— we are not sure whether this is accidental or profound. Figure 9 also shows remarkable agreement between simulation and mean-field results at low density. Since mean field is not so good for the self-correlation at densities around $\rho^* \sim 0.25$ (although it has the right $\rho \to 0$ limit) [see Fig. 2(d)] the good agreement in that range must be due to compensation from the pair interaction part. Finally, we note the good agreement between the $[g_+(r)+g_-(r)]$ obtained from the simulations and the hard-sphere classical $g(r)$ (approximated by the Percus-Yevick g) at $\beta J=0.35$ and $\rho^*=0.55$, shown in Fig. 6(d).

In summary, the equilibrium properties of our model system can be well approximated by relatively simple analytical expressions in both the low- and high-density regions. In particular, they seem to actually improve with ω_0, unlike the semiclassical approximation of Ref. 5. It would certainly be useful to develop similarly good approximations for truly dynamic quantities such as the frequency-dependent susceptibility $\chi(\omega)$; cf. Sec. 4.2 in Ref. 16. This quantity gives direct information about the absorption spectrum of the system and hence also about "localization in one of the potential wells," $\sigma_z=\pm 1$, as a function of the density. The computation can be readily done to low order in the virial expansion or in mean-field theory: it involves, Ref. 16, the evaluation of the Fourier transform of

$$\int_0^\beta \langle \sigma_i^y(0)\sigma_j^z(\lambda+it)\rangle d\lambda \ .$$

Unfortunately, neither of these schemes seems directly useful. In the mean-field theory

$$\chi(\omega) \sim a(\rho)\delta(\omega-\Delta(0))+b(\rho)\delta(\omega) \ ,$$

with $b=0$ for ρ less than the transition density. In the virial expansion to the kth order we can expect to get δ functions corresponding to a system with 2^k levels. It would be very interesting, however, to see if the analog of (2.17), including possibly some sort of broadening around the "pair levels," would still be useful here. We hope to explore this further.

ACKNOWLEDGMENTS

During the course of this work we benefited from discussions and correspondence with Pietro Ballone, David Chandler, Mal Kalos, Michael Klein, Oliver Penrose, Herbert Spohn, and Richard Stratt. Pietro Ballone participated in the early parts of this work. Many of the computations were done on the John von Neumann Center (JvNC) Cyber 205. P.d.S., J.L.L., and J.T. were supported in part by U.S. Air Force Office of Scientific Research, Air Force Systems Command, Department of the Air Force, Grant No. 86-0010. P.N. was supported by National Science Foundation Grant No. 86-12369, a John von Neumann Supercomputer Grant, and the Deutsche Forschungsgemeinschaft.

---

*Present address: Koninklijke Laboratoria Shell, Amsterdam, The Netherlands.

†Also at Department of Physics, Rutgers University, New Brunswick, NJ 08903.

‡Present address: Department of Chemistry and Biochemistry, University of California at Los Angeles, Los Angeles, CA 90024.

[1]D. Chandler and P. G. Wolynes, J. Chem. Phys. **74**, 4078 (1981); K. S. Schweizer, R. M. Stratt, D. Chandler, and P. G. Wolynes, *ibid.* **75**, 1347 (1981); D. Chandler and L. R. Pratt, *ibid.* **65**, 2925 (1976); M. J. Thompson, K. S. Schweizer, and D. Chandler, *ibid.* **76**, 1128 (1982); D. Chandler, K. S. Schweizer, and P. G. Wolynes, Phys. Rev. Lett. **49**, 1100 (1982).

[2]J. S. Hoye and G. Stell, Phys. Rev. Lett. **36**, 1569 (1976); J. Chem. Phys. **75**, 5133 (1981); E. Martina and G. Stell, J. Stat. Phys. **27**, 407 (1982); S. L. Carnie and G. Stell, Phys. Rev. B **26**, 1389 (1982); P. T. Cummings and G. Stell, Mol. Phys. **43**, 1267 (1981).

[3]R. M. Stratt, J. Chem. Phys. **80**, 5764 (1984); Phys. Rev. Lett. **53**, 1305 (1984); S. G. Desjardins and R. M. Stratt, J. Chem. Phys. **81**, 6232 (1984).

[4]R. W. Hall and P. G. Wolynes, J. Stat Phys. **43**, 935 (1986); Phys. Rev. B **33**, 7879 (1986).

[5]P. Ballone, Ph. de Smedt, J. L. Lebowitz, J. Talbot, and E. Waisman, Phys. Rev. A **35**, 942 (1987).

[6]R. B. Stinchcombe, J. Phys. C **6**, 2459 (1973); D. C. Mattis, *The Theory of Magnetism II* (Springer-Verlag, Berlin, 1985).

[7]M. W. Klein, Phys. Rev. B **35**, 1397 (1987).

[8]M. Suzuki, Prog. Theor. Phys. **46**, 1337 (1971); Commun. Math. Phys. **51**, 183 (1976); Prog. Theor. Phys. **56**, 1454 (1976).

[9]D. F. Coker, B. J. Berne, and D. Thirumalai, J. Chem. Phys. **86**, 5689 (1987); M. F. Herman and B. J. Berne, *ibid.* **78**, 4103 (1983); R. A. Chiles, G. A. Jongeward, M. A. Bolton, and P. G. Wolynes, *ibid.* **81**, 2039 (1984); M. Parrinello and A. Rah-

man, *ibid.* **80**, 860 (1984); D. Chandler, Y. Singh, and D. M. Richardson, *ibid.* **81**, 1975 (1984); J. S. Hoye and K. Olaussen, *ibid.* **77**, 2583 (1982).

[10]Proceedings of the Conference of Frontiers of Quantum Monte Carlo, Los Alamos, 1985 [J. Stat Phys. **43**, (1986)]; *Quantum Monte Carlo Methods,* edited by M. Suzuki (Springer-Verlag, Berlin, 1987); *Monte Carlo Methods in Quantum Problems,* edited by M. H. Kalos (Plenum, New York, 1982); D. Chandler, *Introduction to Modern Statistical Mechanics* (Oxford University Press, New York, 1987).

[11]For the "classical" theory, cf. T. L. Hill, *Statistical Mechanics* (McGraw-Hill, New York, 1956); and articles by J. Percus, G. Stell, and others in *Classical Fluids,* edited by H. L. Frisch and J. L. Lebowitz (Benjamin, New York, 1964). For the "modern" version, cf. D. Brydges and T. Kennedy, J. Stat Phys. **48**, 19 (1987).

[12]J. L. Lebowitz and O. Penrose, J. Math. Phys. **4**, 1312 (1963).

[13]J. Ginibre, J. Math. Phys. **6**, 238 (1965); **6**, 256 (1965); **6**, 1432 (1965); D. Ruelle, *Statistical Mechanics* (Benjamin, New York, 1969).

[14]H. Spohn and R. Dümke, J. Stat. Phys. **41**, 389 (1985).

[15]M. W. Klein, Phys. Rev. B **29**, 5825 (1984).

[16]R. Kubo, M. Toda, and N. Hashitsume, *Statistical Physics II* (Springer-Verlag, Berlin, 1985).

[17]M. Fannes, H. Spohn, and A. Verbeure, J. Math. Phys. **21**, 355 (1980).

[18]N. N. Bogoliubov, Jr., *A Method for Studying Model Hamiltonians* (Pergamon, New York, 1972).

[19]Compare Eqs. (4.1.11)–(4.1.14) in Ref. 16.